Oxygen and aluminum tracer diffusion in (−201) oriented β-Ga_2O_3 single crystals

Johanna Uhlendorf[1] and Harald Schmidt[1,2,*]

[1]Technische Universität Clausthal, Institut für Metallurgie, AG Festkörperkinetik, 38678 Clausthal-Zellerfeld, Germany
[2]Clausthaler Zentrum für Materialtechnik, Technische Universität Clausthal, 38678 Clausthal-Zellerfeld, Germany

(Received 26 May 2023; accepted 14 September 2023; published 29 September 2023)

β-Ga_2O_3 is an ultrawide band-gap semiconductor with importance for various technological applications. We investigated the tracer diffusion of oxygen and aluminum (as a substitute tracer for gallium) in (−201) oriented β-Ga_2O_3 single crystals between 1100 and 1600 °C. Isotope enriched $^{18}O_2$ gas or ion-beam sputtered thin films of Al_2O_3 were used as a tracer source. The isotope depth profiles were analyzed by secondary ion mass spectrometry. The Al diffusivities are by two orders of magnitude higher than the O diffusivities. Activation enthalpies of diffusion of about 4.2 eV for Al and 5.0 eV for O were derived. Possible diffusion mechanisms are discussed in the framework of density functional theory calculations as known from the literature. As a result, O interstitials and Ga vacancies are suggested as defects governing diffusion.

DOI: 10.1103/PhysRevMaterials.7.093402

I. INTRODUCTION

The β phase of gallium oxide is an ultrawide band-gap semiconductor with a band gap of 4.6–4.9 eV [1]. Due to its multifunctional use in diverse applications this material is becoming increasingly important in various fields of technology [2–11]. Examples are power electronic devices [3,4,12,13], gas sensing [2,14,15], and solar blind UV photodetection [3]. β-Ga_2O_3 is optically transparent to wavelengths of about 260 nm and is also electrically conducting [10], making it useful as a window on special types of optical devices [3].

The electrical conductivity σ of nominally undoped β-Ga_2O_3 crystals can be attributed to unintentional dopants such as silicon, tin, and/or hydrogen [11,16,17] and it depends on the oxygen partial pressure by $\sigma \sim p_{O2}^{-1/4}$ [18]. The material can be n doped (Si or Sn) up to 10^{20} cm^3 leading to an increase of electrical conductivity [3,17,19–22]. It should be noted that at the moment the understanding of doping and of the underlying mechanisms (preferential n doping and lack of p dopants) is currently in the early stage and there is still no widespread agreement [5,23–26].

The knowledge and study of native point defects [5,26,27] and their migration play an important role in the fundamental understanding of the electrical and optical properties of β-Ga_2O_3. Point defects are always present in materials and they are introduced into the material either during crystal growth or afterwards during postgrowth heat treatment. Bulk transport of the ionic species is also expected to control redox kinetics at the surface [2]. Self-diffusion experiments will give information on possible native defects present in the material and their mobility as a function of temperature. In addition, self-diffusion processes are also essential for homogenization and/or modification of the native stoichiometry of crystals.

Several theoretical papers have been published on point defects, diffusion, and their energetics [1,2,11,13,16,25,26,28–32]. *Ab initio* calculations on β-Ga_2O_3 are time consuming due to the low symmetry of the monoclinic crystal lattice but also due to the ambiguity in the determination of the interstitial sites and the migration paths [28]. Consequently, information on defects and defect energies, which are determined from experimental studies, are important for an overall understanding. One of these experimental studies are tracer diffusion experiments as described in the present paper. The basic aim is to provide diffusion parameters for O and Ga in β-Ga_2O_3 single crystals. Oxygen diffusion can be traced using stable $^{18}O_2$ tracers with a natural abundance of only 0.2%. In order to measure Ga self-diffusion in principle two stable tracer atoms are available, ^{69}Ga and ^{71}Ga, with relative abundances of 60.1% and 39.9% respectively. Due to this isotope composition, neither of the two isotopes can be used as a tracer because the natural abundance in ^{nat}Ga is too high for each. The in-diffusion of the tracer for a detailed analysis would simply not be visible and will be masked by the background of ^{nat}Ga. Consequently, Al (^{27}Al) will be used as a substitute tracer [33]. It is in the same main group in the periodic system as Ga (valence isoelectronic) and the compound β-Al_2O_3 is stable also in a different temperature/pressure domain. Even if the diffusivities of Al are not expected to be absolutely identical to those of Ga, the results will be similar and basic quantities (activation energy, diffusivities) can be derived in direct comparison to oxygen diffusion. Therefore, the aim of the paper is to investigate the diffusion of Al and O in β-Ga_2O_3. The analysis of the diffusion results in Sec. IV, which is partly based on the migration of Ga ions, must be handled with caution. However, respective data on Al migration in bulk β-Ga_2O_3 have not yet been published up to now. Note that conclusions about the doping properties of Ga cannot be derived easily from the experimental data of Al.

II. EXPERIMENT DETAILS

The β-Ga_2O_3 single crystals under investigation were obtained from Novel Crystal Technology, Inc., Japan and are

*Corresponding author: harald.schmidt@tu-clausthal.de

 ©2023 American Physical Society

referred to as unintentionally doped. The crystals were grown by the edge-defined film-fed method as described in [34]. For the diffusion experiments, wafers of $5\times5\times0.5\,\mathrm{mm}^3$ were cut from the crystal and were chemical-mechanically polished. The surface orientation of the investigated wafers is (-201). Crystals produced with the given method normally have a low impurity concentration, while the impurities with the highest concentration are Si (2.3 wt ppm), Ir (4.9 wt ppm), and Al and Fe (0.81 wt ppm) according to a publication of the suppliers [34]. Contamination with hydrogen does not play a significant role here, because our experiments were carried out at high temperatures in oxygen [22]. The as-received crystals were cleaned in isopropanol for several minutes.

Prior to the actual diffusion experiments, the crystals were isothermally pre-annealed in natural oxygen (99.8% $^{16}O_2$) gas at 200 mbar for a period considerably longer than the actual diffusion time, to achieve thermodynamic and defect equilibrium at the given temperature, at least at the surface. The samples were placed on an alumina (Al_2O_3) holder connected to a mechanical feed-through manipulator, allowing a rapid insertion and removal of the sample holder into the hot zone of a resistance tube furnace within 5 min, or to withdraw it, respectively.

Actual oxygen diffusion experiments were carried out by further annealing the pre-annealed samples in $^{18}O_2$ enriched gas. The exact isotope $^{18}O_2$ gas concentration in the furnace was measured by a residual gas analyzer (RGA 200, Stanford Research Systems) to be about 94%. During diffusion annealing isotope exchange between ^{16}O and ^{18}O takes place.

Concerning Al diffusion, tracer deposition was carried out by placing a thin layer of Al_2O_3 on top of the β-Ga_2O_3 single crystals by ion beam sputtering. Ion-beam sputtering was done using a commercial setup (IBC 681, Gatan) equipped with two penning ion sources at a 45° beam angle, positioned about 10 cm above the sample. The base pressure of the vacuum chamber was 5×10^{-7} mbar. Deposition was done at 5 keV and at 200 μA using argon sputter gas at an operation pressure of 5×10^{-3} mbar. During deposition, the specimen is rotated (30 rotations per minute) and rocked (rock angle: 30°; rock speed: 12° per second) to ensure a uniform coating of the sample. Commercially available high purity sapphire crystals (Crystec, Berlin) were used as sputter targets. For the diffusion experiments the prepared β-Ga_2O_3 single crystals with sputtered Al_2O_3 tracer layer on top were annealed in natural oxygen atmosphere (200 mbar) at the respective temperatures as described above. After annealing the samples were stored in a desiccator. Information on temperatures, times, and corresponding diffusivities are given in the Supplemental Material [35].

Isotope depth profile analysis was done by secondary ion mass spectrometry (SIMS) using a Cameca ims-$3f/4f$ instrument. An O^- primary ion beam (14.5 keV, 80 nA) was used. The sputtered area was about 250 μm × 250 μm wherefrom 20% in the center was gated for further signal processing in a double focused mass spectrometer. In depth profiling mode, the secondary ion intensities of $^{16}O^+$, $^{18}O^+$, $^{27}Al^+$, $^{69}Ga^+$, and $^{71}Ga^+$ ions were recorded as a function of sputtering time. Depth calibration was obtained by measuring the crater depth with a mechanical surface profiler (Tencor, Alphastep).

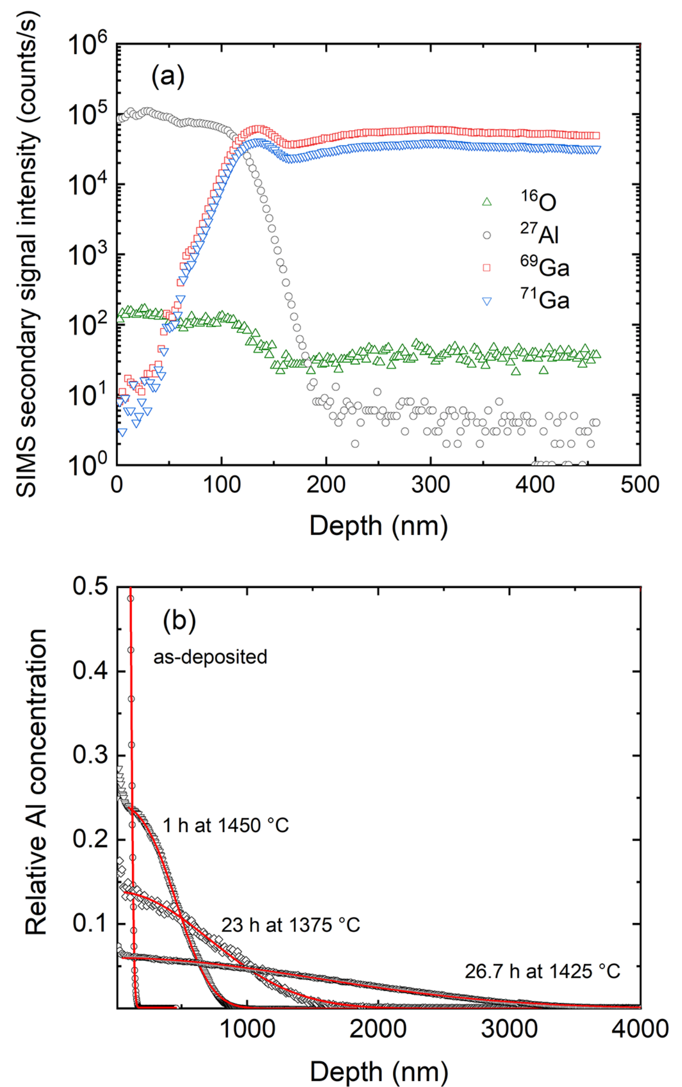

FIG. 1. (a) SIMS secondary ion intensities of a β-Ga_2O_3 single crystal with a tracer layer after deposition (logarithmic scaling). (b) Relative Al concentration as a function of depth for an as-deposited sample and samples annealed at different temperatures in O_2 (dots). Also shown are fitting curves according to Eq. (1) as lines.

III. RESULTS

First, the experiments on Al diffusion are discussed. Figure 1(a) shows SIMS secondary ion intensities of a sample after pre-annealing and tracer deposition. The Al_2O_3 sputter layer is clearly visible by the decrease of the Al signal and the simultaneous increase of the ^{69}Ga and ^{71}Ga signals. The maximum intensity of Al and the sum of the two Ga isotopes is approximately identical, indicating that the ionization probability of these elements is similar.

In Fig. 1(b) the relative Al concentration in β-Ga_2O_3 as obtained from SIMS depth profile analysis before and after diffusion annealing at different temperatures is displayed as examples. The SIMS signals of the annealed samples were normalized to the background level of the as-deposited sample at large depths. A broadening of the initial thin layer to the micrometer range during annealing is indicated.

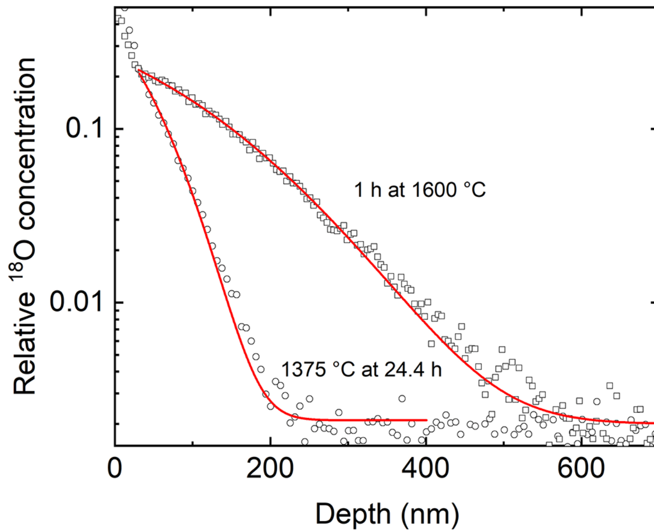

FIG. 2. Relative ^{18}O fraction as a function of depth for samples after $^{18}O_2$ exchange at 1375 °C and 1600 °C respectively. Also shown are fitting curves according to Eq. (2).

Without any diffusion annealing the depth profile can be fitted using the thick film solution to Fick's second law pertaining to diffusion across an interface [36],

$$c(x,t) = c_\infty + \frac{1}{2}(c_0 - c_\infty)\left[\mathrm{erf}\left(\frac{h+x}{R}\right) + \mathrm{erf}\left(\frac{h-x}{R}\right)\right] \quad (1)$$

with $c_0 \approx 1$ being the relative Al concentration present in the top layer, $c_\infty \approx 0$ being the relative Al concentration in the background, h being the thickness of the Al_2O_3 sputter layer (about 150–300 nm depending on the experiment), and $R = R_0 = 20$ nm being the "width" of the aluminum distribution at the interface. The diffusion annealed samples were also fitted by Eq. (1) in order to determine the aluminum tracer diffusivities. The Al diffusivity D_{Al} is determined from the difference in the respective broadening R of the Al distribution of the diffusion profile and of the as-deposited profile R_0 according to $D_{\mathrm{Al}} = (R^2 - R_0^2)/4t$, where t is the annealing time [37]. The fitting result is displayed as continuous red lines in Fig. 1(b). The error limits of about 40% attributed to each diffusivity result from the uncertainty in the crater depth determination, from fitting error, and from the measurement at different locations on the sample surface. Diffusion experiments were carried out in the temperature range between 1100 °C and 1450 °C.

In Fig. 2 examples of O diffusion experiments are illustrated. We see the relative ^{18}O isotope fraction in β-Ga_2O_3 as obtained from SIMS depth profile analysis after $^{18}O_2/^{16}O_2$ isotope-exchange annealing exemplarily at 1375 °C and 1600 °C, respectively. The penetration of the ^{18}O tracer from the gas phase into the crystal is clearly seen. The following solution of the diffusion equation for a constant gas source was used to evaluate the diffusivities [36]:

$$c(x,t) = c_\infty + (c_0 - c_\infty)\mathrm{erfc}\left(\frac{x}{2\sqrt{D_{Ox}\,t}}\right), \quad (2)$$

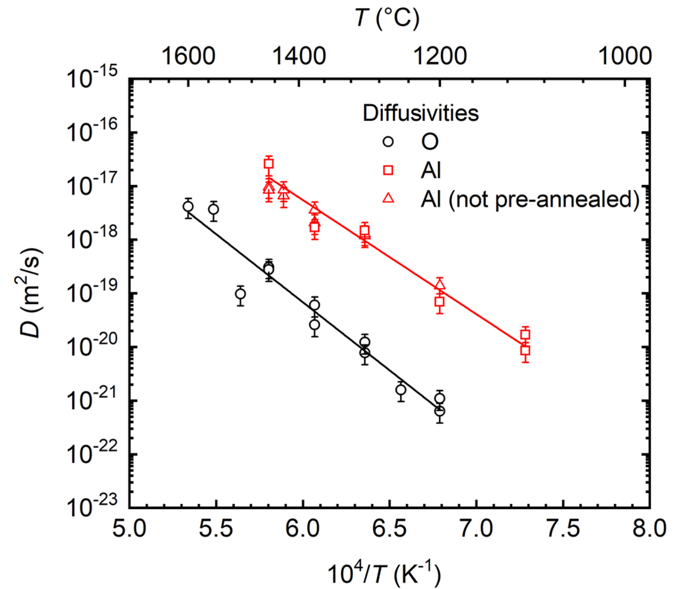

FIG. 3. Al diffusivities and O diffusivities in β-Ga_2O_3 (−201 orientation) as a function of reciprocal temperature as obtained by tracer diffusion measurements using SIMS.

where c_0 is the ^{18}O isotope fraction at the surface and $c_\infty = 0.002$ is the background ^{18}O isotope fraction, D_{Ox} is the oxygen diffusivity, and t is the annealing time. The unchanged signal during annealing in the region less than 50 nm below the surface is probably due to the formation of a thin electrically insulating layer after annealing bulk β-Ga_2O_3 samples at high temperatures in the presence of oxygen [21]. It is also observed for the Al diffusion experiments and not used for analysis. The diffusion experiments were carried out in the temperature range 1200−1600 °C.

In Fig. 3 the determined tracer diffusivities of both species are plotted as a function of the reciprocal temperature. For Al diffusion, experiments were carried out on pre-annealed and not pre-annealed samples. The diffusivities are identical within error limits. The Al diffusivities are about two orders of magnitude higher than the O diffusivities measured on the same type of samples. Both types of diffusivity obey the Arrhenius law,

$$D = D_0 \exp(-\Delta H/kT), \quad (3)$$

where ΔH is the activation enthalpy of diffusion and D_0 is the pre-exponential factor. A least-squares fit of Eq. (3) to the diffusivities of each species gives an activation enthalpy of $\Delta H_{\mathrm{Ox}} = 5.0 \pm 0.4$ eV and a pre-exponential factor of $D_{0,\mathrm{Ox}} = 1.1 \times 10^{-4}$ m^2/s (error: ln $D_{0,\mathrm{O}}$/m^2/s $= -9.0 \pm 2.7$) for oxygen and $\Delta H_{\mathrm{Al}} = 4.2 \pm 0.4$ eV and $D_{0,\mathrm{Al}} = 3.2 \times 10^{-5}$ m^2/s (error: ln $D_{0,\mathrm{Al}}$/m^2/s $= -10.3 \pm 3.2$) for aluminum (pre-annealed and not pre-annealed samples fitted together). The activation enthalpy of Al is about 1 eV lower than that of O, which is the main reason for the higher diffusivities.

Regarding oxygen diffusion, diffusivities have already been determined by our group on (100) oriented single crystals obtained from Institut für Kristallzüchtung (IKZ), Berlin [38], which are shown in Fig. 4 in comparison to the actual

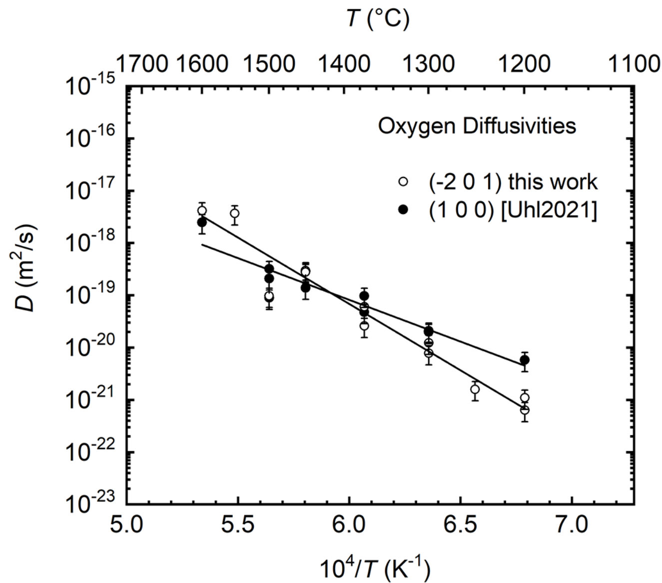

FIG. 4. O diffusivities in β-Ga_2O_3 as a function of reciprocal temperature as obtained by tracer diffusion measurements using SIMS. Shown are the diffusivities obtained in this work on (−201) oriented crystals and those of Ref. [38] [Uhl2021] on (100) oriented crystals. Note that both types of crystals may have different impurity levels (see discussion in Sec. IV).

data set. The diffusivities are very similar for temperatures above 1300 °C. However, there is a discrepancy at lower temperatures. The oxygen diffusivities of (−201) oriented crystals are lower by almost one order of magnitude at 1200 °C. By fitting with Eq. (3) this leads to a higher activation energy of diffusion, 5.0 ± 0.4 eV instead of 3.2 ± 0.4 eV. This result is unexpected and probably indicates different migration paths of oxygen (see discussion below) and the result might be due to the different orientation of the crystals. Alternatively, it could be also due to a different level of impurity defects in the crystals (see discussion below). Clearly, more detailed measurements are needed in the future to clarify this. However, it should also be noted that there is a significant scatter of data, even for the same temperature. This results in relatively high error limits of the activation enthalpies of about 0.4 eV, which might explain a part of the difference.

IV. DISCUSSION

In general, for line compounds such as β-Ga_2O_3 with a small stability range, two enthalpies may contribute to the overall activation enthalpy of diffusion ΔH. These are the enthalpy of migration via a certain defect (vacancy or interstitial) ΔH_m, and the enthalpy of formation of the respective defect ΔH_f. This is valid for both types of diffusors. For further discussion, it is assumed that the terms formation/migration energy and enthalpy are identical in good approximation. We first focus on the diffusion of Al as a substitute tracer for Ga and assume that Al diffuses on Ga lattice sites. A straightforward way to analyze experimentally derived activation energies is a comparison to formation and migration energies derived by *ab initio* computer calculations. Such a comparison has to be done with caution because theoretically calculated energies may not necessarily apply to real systems, investigated experimentally. Computer calculations of migration and formation energies are available for Ga and O based defects in the literature. Unfortunately, migration energies for Al (e.g., Al-vacancy exchange) in bulk β-Ga_2O_3 have not been published up to now (only for surface adsorption and migration [31]) and we have to use the data of Ga as an approximation. The comparison between experimental and theoretical data should be seen as a basic idea how diffusion may take place in β-Ga_2O_3 and not as a rigid proof. Consequently, different possibilities are discussed.

In principle, gallium vacancies or interstitials are possible as characteristic and simple point defects governing diffusion. Kyrtsos *et al.* [2] calculated the migration barriers of gallium vacancies (vacancy-Ga exchange as an approximation to Al) by nudged elastic band and dimer methods within the standard density functional theory (DFT). Due to the monoclinic structure of gallium oxide there exist two gallium sites and several different diffusion paths have to be considered. Migration barriers for single ion jumps between 0.6 and 2.2 eV were found for threefold positively charged gallium vacancies. Recently, Frodason and co-workers [30] did similar work with nudged elastic band methods and deduced from local migration barriers the migration energies necessary for long range diffusion in (100) and (010) direction to 2.08 eV and in (001) direction to 0.97 eV introducing three split vacancies. Consequently, for the (−201) crystal orientation under investigation in this work, a migration energy of about 2.1 eV can be expected for Ga vacancies. For Ga interstitials the overall migration barrier is less, namely about 1.0 eV. Both values are significantly lower than the experimentally determined activation energy of diffusion of 4.2 eV. Consequently, a defect formation part is necessary to explain our results if we exclude the possibility that the calculations give too low values.

Concerning defect formation energies, Zacherle and coworkers carried out *ab initio* calculations based on density functional theory using the HSE06 exchange integral [11]. For high oxygen partial pressures and undoped samples (the Fermi energy is close to the middle of the band gap) they calculated formation energies of 6 V for gallium interstitials and 4 eV for gallium vacancies. References [2,26] found similar values. Adding the migration and formation energy, we obtain an overall activation energy of about 6 eV for vacancies and of 7 eV for interstitials, which is not compatible with the experimental results.

As stated above, we may have some impurities in the crystal due to unintentional doping. This may also influence defect formation energies. According to the most plausible scenario for point defects in unintentionally doped β-Ga_2O_3 crystals, a low-level donor doping by tetravalent atoms such as Si or others is unavoidable and responsible for the *n*-type conductivity [11,16,17]. Small amounts of impurity donors of some ppm may dominate the defect structure. In our type of crystals the tetravalent donor impurity with the highest concentration is silicon which is present in a concentration of $\sim 3 \times 10^{17}$ cm^{-3} (3 ppm) [34] according to glow discharge mass spectrometry measurements (iridium is expected to be a deep donor [39] or trivalent). This is a low value, but assuming that this is only an estimation for the crystals under investigation here, an influence on the defect structure cannot

be excluded. According to DFT calculations in Ref. [11], the Fermi level is shifted closer to the conduction band for tetravalent donor doping of only 10 ppm. This leads to an increase of the formation energies of interstitials and a decrease of the formation energies of vacancies, which makes interstitials as defects governing diffusion unlikely. For a calculated Fermi level of 3.47 eV corresponding to doping of 10 ppm [11], a formation energy of about only 1 eV can be expected for gallium vacancies in the dilute limit. Since the exact location of the Fermi level for our doping concentration is not known, we assume a formation energy between 1 and 4 eV. Adding a formation energy of 2 eV and a migration energy of 2 eV, the measured activation energy of diffusion of 4 eV is in agreement to these calculations. In Ref. [31] it is calculated that the migration of Ga adatoms on the surface of β-Ga_2O_3 corresponds to a lower energy barrier than that of Al. It is concluded that tetrahedral to octahedral site hopping of Al should also be more difficult in bulk. This will not fundamentally change our analysis. However, the diffusivities of Al might be seen as a lower border for the diffusivities of Ga due to a higher migration energy and consequently activation energy of the Al species.

The presence of Ga vacancies, which are used to explain our results, was proven experimentally by electron paramagnetic resonance measurements [40] and positron annihilation spectroscopy [41,42].

A similar analysis can be done for the diffusion of oxygen. Again, Kyrtsos *et al.* calculated the migration barrier of oxygen vacancies to be between 1.2 and 2.7 eV. For long range diffusion in the (−201) direction it can be expected that the migration barrier is at the higher end of the energy spectrum close to 2.7 eV (see also [30] for Ga vacancy migration). For defect formation energies (HSE06 hybrid functional), Zacherle and co-workers [11] found formation energies of 4 eV for oxygen vacancies and interstitials for high oxygen partial pressures and for the undoped case. Regarding the experimentally found activation energy of diffusion of 5.0 eV, this scenario is also not very likely, but cannot be completely excluded assuming a migration energy below 2 eV. For donor doped samples, an increase of the formation energy of vacancies and a decrease of the formation energies of interstitials are calculated [11,26]. With these data the diffusion of oxygen with an activation energy of 5 eV becomes more likely via interstitials than via vacancies even for low doping concentrations. While diffusion via oxygen vacancies is theoretically possible for the undoped case with a formation energy of 3–4 eV [11,16,26] and a low migration energy of only 1–2 eV, such an assumption contradicts the analysis of Ga/Al diffusion, carried out experimentally on the same type of sample. Indications (theoretically or experimentally) for a possible diffusion of oxygen in the molecular state are not known.

As mentioned above for the measurement on (100) oriented crystals [38], the activation energy of diffusion is lower, which can be explained by a higher doping level of tetravalent donors that shift the formation energy of oxygen interstitials to lower values.

In summary, the experimental results can best be explained by assuming slightly unintentionally donor doped crystals where diffusion takes place via Ga vacancies and O interstitials. This result and the higher diffusivities of Al compared to O are also supported by the direct calculation of the concentration of point defects [11] for donor doped samples at 1000° C and ambient pressure. In general, the higher the defect concentration, the higher the diffusion. The authors found (beneath electrons) the highest concentration of point defects for Ga vacancies, while that of O interstitials is lower, but both above oxygen vacancies. For the undoped case, the highest defect concentration shows oxygen vacancies above gallium vacancies, which is unlikely according to our experimental results. Note that this analysis has to be treated with some caution because it is not excluded that other nontetravalent ions may also influence the defect distribution, at least in part [26,27]. According to Ref. [11], for Fermi energies of the *n*-doped case (higher than 3 eV) the formation energy of oxygen interstitials is always higher than that of Ga vacancies, resulting in a difference of about 1 eV at a Fermi energy of 3.47 eV corresponding to doping of 10 ppm. This is also in good agreement with the difference of the activation energies of diffusion experimentally found in this study.

Differences in diffusivities can often be discussed with regard to ionic radii. According to Shannon [43] the ionic radius of O^{2-} (about 1.4 Å) is higher than that of Al^{3+} (about 0.4−0.5 Å) irrespective of the coordination numbers. We assume that this is also valid for Ga_2O_3, at least in approximation. According to these data, the faster diffusion of Al is reasonable due to the smaller radius. Note that such "size effects" are expected to be inherently included in the theoretical calculations of the migration energies.

The charge state of the ions is expected to be 3+ for Ga and 2− for O. From [11] we see that the charge state of the defects are 2− for the O interstitial and 3− for the Ga vacancy for the unintentionally doped case. This is the lowest energy configuration and a different charge state would correspond to a higher formation energy. However, a modification of the charge state of these defects can be expected for lower Fermi energies which would correspond to undoped or *p*-doped samples which is not the case here.

V. CONCLUSION

In conclusion, we carried out O and Al tracer diffusivity measurements in (−201) oriented β-Ga_2O_3 single crystals using secondary ion mass spectrometry depth profiling. Al is used as a substitute tracer to monitor the migration of Ga. The results of the diffusion experiments show that Al diffusion is two orders of magnitude faster than the O diffusion, while the activation energies are 5.0 eV for oxygen and 4.2 eV for aluminum. Comparison of the experimental result to computational calculations on defect formation and migration energies as given in the literature suggests that the diffusion of Al is governed by gallium vacancies and that of oxygen by interstitials. We assume that defect formation is determined by low unintentional donor doping in the ppm range.

ACKNOWLEDGMENT

This work was funded by the Deutsche Forschungsgemeinschaft (DFG, German Research Foundation) Grant No. SCHM 1569/35-1. The financial support is gratefully acknowledged.

[1] C. Janowitz, V. Scherer, M. Mohamed, A. Krapf, H. Dwelk, R. Manzke, Z. Galazka, R. Uecker, K. Irmscher, R. Fornari, M. Michling, D. Schmeißer, J. R. Weber, J. B. Varley, and C. G. de van Walle, New J. Phys. **13**, 85014 (2011).
[2] A. Kyrtsos, M. Matsubara, and E. Bellotti, Phys. Rev. B **95**, 245202 (2017).
[3] S. J. Pearton, J. Yang, P. H. Cary, F. Ren, J. Kim, M. J. Tadjer, and M. A. Mastro, Appl. Phys. Rev. **5**, 11301 (2018).
[4] S. J. Pearton, F. Ren, M. Tadjer, and J. Kim, J. Appl. Phys. **124**, 220901 (2018).
[5] M. J. Tadjer, J. L. Lyons, N. Nepal, J. A. Freitas, A. D. Koehler, and G. M. Foster, ECS J. Solid State Sci. Technol. **8**, Q3187 (2019).
[6] S. Stepanov, V. Nikolaev, V. E. Bougrov, and A. E. Romanov, Rev. Mater. Sci. **44**, 63 (2016).
[7] M. Razeghi, J.-H. Park, R. McClintock, D. Pavlidis, F. H. Teherani, D. J. Rogers, B. A. Magill, G. A. Khodaparas, Y. Xu, J. Wu, and V. P. Dravid, SPIE Proc. **10533**, 105330R (2018).
[8] S. Pearton, M. Mastro, and F. Ren, *Gallium Oxide - Technology, Devices and Applications* (Elsevier, San Diego, 2018).
[9] Y.-W. Huan, S.-M. Sun, C.-J. Gu, W.-J. Liu, S.-J. Ding, H.-Y. Yu, C.-T. Xia, and D. W. Zhang, Nanoscale Res. Lett. **13**, 246 (2018).
[10] Z. Galazka, Semicond. Sci. Technol. **33**, 113001 (2018).
[11] T. Zacherle, P. C. Schmidt, and M. Martin, Phys. Rev. B **87**, 235206 (2013).
[12] M. Higashiwaki, K. Sasaki, A. Kuramata, T. Masui, and S. Yamakoshi, Appl. Phys. Lett. **100**, 13504 (2012).
[13] M. A. Mastro, A. Kuramata, J. Calkins, J. Kim, F. Ren, and S. J. Pearton, ECS J. Solid State Sci. Technol. **6**, P356 (2017).
[14] T. Weh, J. Frank, M. Fleischer, and H. Meixner, Sens. Actuators B **78**, 202 (2001).
[15] A. Trinchi, W. Wlodarski, and Y. X. Li, Sensor. Actuators B **100**, 94 (2004).
[16] J. B. Varley, J. R. Weber, A. Janotti, and C. G. van de Walle, Appl. Phys. Lett. **97**, 142106 (2010).
[17] E. G. Víllora, K. Shimamura, Y. Yoshikawa, T. Ujiie, and K. Aoki, Appl. Phys. Lett. **92**, 202120 (2008).
[18] M. Fleischer and H. Meixner, Sensor. Actuators B **4**, 437 (1991).
[19] N. Ueda, H. Hosono, R. Waseda, and H. Kawazoe, Appl. Phys. Lett. **70**, 3561 (1997).
[20] S. Müller, H. von Wenckstern, D. Splith, F. Schmidt, and M. Grundmann, Phys. Status Solidi A **211**, 34 (2014).
[21] Z. Galazka, K. Irmscher, R. Uecker, R. Bertram, M. Pietsch, A. Kwasniewski, M. Naumann, T. Schulz, R. Schewski, D. Klimm, and M. Bickermann, J. Cryst. Growth **404**, 184 (2014).
[22] Z. Galazka, K. Irmscher, R. Schewski, I. M. Hanke, M. Pietsch, S. Ganschow, D. Klimm, A. Dittmar, A. Fiedler, T. Schroeder, and M. Bickermann, J. Cryst. Growth **529**, 125297 (2020).
[23] C. J. Zeman, S. M. Kielar, L. O. Jones, M. A. Mosquera, and G. C. Schatz, J. Alloy. Compd. **877**, 160227 (2021).
[24] J. Zhang, J. Shi, D.-C. Qi, L. Chen, and K. H. L. Zhang, APL Mater. **8**, 020906 (2020).
[25] R. Sharma, M. E. Law, F. Ren, A. Y. Polyakov, and S. J. Pearton, J. Vac. Sci. Technol. A **39**, 060801 (2021).
[26] H. Peelaers, J. L. Lyons, J. B. Varley, and C. G. van de Walle, APL Mater. **7**, 22519 (2019).
[27] M. D. McCluskey, J. Appl. Phys. **127**, 101101 (2020).
[28] M. A. Blanco, M. B. Sahariah, H. Jiang, A. Costales, and R. Pandey, Phys. Rev. B **72**, 184103 (2005).
[29] L. Dong, R. Jia, C. Li, B. Xin, and Y. Zhang, J. Alloy. Compd. **712**, 379 (2017).
[30] Y. K. Frodason, J. B. Varley, K. M. H. Johansen, L. Vines, and C. G. van de Walle, Phys. Rev. B **107**, 024109 (2023).
[31] M. Wang, S. Mu, and C. G. van de Walle, ACS Appl. Mater. Inter. **13**, 10650 (2021).
[32] A. Usseinov, Z. Koishybayeva, A. Platonenko, V. Pankratov, Y. Suchikova, A. Akilbekov, M. Zdorovets, J. Purans, and A. I. Popov, Materials **14**, 7384 (2021).
[33] C. Herzig, M. Friesel, D. Derdau, and S. V. Divinski, Intermetallics **7**, 1141 (1999).
[34] A. Kuramata, K. Koshi, S. Watanabe, Y. Yamaoka, T. Masui, and S. Yamakoshi, Jpn. J. Appl. Phys. **55**, 1202A2 (2016).
[35] See Supplemental Material at http://link.aps.org/supplemental/10.1103/PhysRevMaterials.7.093402 for temperatures, times, and corresponding diffusivities of all samples investigated.
[36] J. Crank, *The Mathematics of Diffusion*, 2nd ed., reprinted (Oxford University Press, Oxford, 2009).
[37] J. Rahn, E. Hüger, L. Dörrer, B. Ruprecht, P. Heitjans, and H. Schmidt, Phys. Chem. Chem. Phys. **14**, 2427 (2012).
[38] J. Uhlendorf, Z. Galazka, and H. Schmidt, Appl. Phys. Lett. **119**, 242106 (2021).
[39] C. A. Lenyk, N. C. Giles, E. M. Scherrer, B. E. Kananen, L. E. Halliburton, K. T. Stevens, G. K. Foundos, J. D. Blevins, D. L. Dorsey, and S. Mou, J. Appl. Phys. **125**, 45703 (2019).
[40] B. E. Kananen, L. E. Halliburton, K. T. Stevens, G. K. Foundos, and N. C. Giles, Appl. Phys. Lett. **110**, 202104 (2017).
[41] F. Tuomisto, Jpn. J. Appl. Phys. **62**, SF0802 (2023).
[42] E. Korhonen, F. Tuomisto, D. Gogova, G. Wagner, M. Baldini, Z. Galazka, R. Schewski, and M. Albrecht, Appl. Phys. Lett. **106**, 242103 (2015).
[43] R. D. Shannon, Acta Cryst. A **32**, 751 (1976).